Journal of Molecular Graphics and Modelling 29 (2011) 597–607

Contents lists available at ScienceDirect

Journal of Molecular Graphics and Modelling

journal homepage: www.elsevier.com/locate/JMGM

Inhibition of peptide aggregation by lipids: Insights from coarse-grained molecular simulations

Andrew Hung*, Irene Yarovsky

Health Innovations Research Institute and School of Applied Sciences, RMIT University, GPO Box 2476V, Melbourne, Victoria 3001, Australia

ARTICLE INFO

Article history:
Received 24 March 2010
Received in revised form 30 October 2010
Accepted 1 November 2010
Available online 11 November 2010

Keywords:
Peptide
Aggregation
Amyloid
Molecular dynamics
Simulation
Lipids
Apolipoprotein
Coarse-grained

ABSTRACT

The amyloidogenic peptide apolipoprotein C-II(60–70) is known to exhibit lipid-dependent aggregation behaviour. While the peptide rapidly forms amyloid fibrils in solution, fibrillisation is completely inhibited in the presence of lipids. In order to obtain molecular-level insights into the mechanism of lipid-dependent fibril inhibition, we have employed molecular dynamics simulations in conjunction with a coarse-grained model to study the aggregation of an amyloidogenic peptide, apoC-II(60–70), in the absence and presence of a short-chained lipid, dihexanoylphosphatidylcholine (DHPC). Simulation of a solution of initially dispersed peptides predicts the rapid formation of an elongated aggregate with an internal hydrophobic core, while charged sidechains and termini are solvent-exposed. Inter-peptide interactions between aromatic residues serve as the principal driving force for aggregation. In contrast, simulation of a mixed peptide–DHPC solution predicts markedly reduced peptide aggregation kinetics, with subsequent formation of a suspension of aggregates composed of smaller peptide oligomers partially inserted into lipid micelles. Both effects are caused by strong interactions between the aromatic residues of the peptide with the lipid hydrophobic tails. This suggests that lipid-induced aggregate inhibition is partly due to the preferential binding of peptide aromatic sidechains with lipid hydrophobic tails, reducing inter-peptide hydrophobic interactions. Furthermore, our simulations suggest that the morphology of peptide aggregates is strongly dependent on their local lipid environment, with greater contacts with lipids resulting in the formation of more elongated aggregates. Finally, we find that peptides disrupt lipid self-assembly, which has possible implications for explaining the cytotoxicity of peptide oligomers.

1. Introduction

A number of debilitating human disorders are characterised by the extracellular deposition of insoluble aggregates composed of proteins and other biomolecules in the body, including Alzheimer's, Parkinson's, Huntington's and the transmissible prion diseases [1]. Numerous experimental evidence now indicates that many sequentially and structurally non-homologous proteins and peptides, as yet un-associated with any known physiological disorders, are capable of fibril-formation given certain environmental conditions, such as pH, temperature, pressure and ionic strength [2,3]. In addition to full-length proteins, "core fibril regions" within intact proteins have been identified using computational techniques [4]. These derivative peptides, when cleaved from the full-length chain, have been shown to be capable of independent fibril formation. Examples include short peptides derived from islet amyloid polypeptide (IAPP) [5], the central motif of human calcitonin [6], fibril-forming segments of yeast prion protein sup35 [7], 21-residue [8] and 11-residue [9] fragments of human apolipoprotein C-II (apo-CII). Understanding the aggregation mechanism of amyloidogenic derivative peptides is important due to the possible insights that may be obtained into the fundamental fibrillisation principles of larger proteins.

Conversely, conditions may be contrived which inhibit the formation of insoluble aggregates and, in some cases, result in the dissociation of mature fibrils. Examples include oxidation [10,11] and binding to cyclic organic molecules (cyclodextrin) [12,13] and peptides [14]. More recent work have also indicated the role of surfactants and lipids in regulating the morphology of mature fibrils formed from human apolipoprotein C-II [8], as well as their formation kinetics, in some cases fully inhibiting their formation [8]. Phosphocholine (PC) lipids is known to inhibit fibrillisation of apoC-II protein and its fibrillogenic tryptic peptides, apoC-II(56–76) [15,16] and apoC-II(60–70) [9,17], in a concentration-dependant manner.

Theoretical molecular modelling is long-recognised as a powerful complement to experimental studies in the biological sciences, and has been employed to study protein aggregation. We have previously applied all-atom molecular dynamics (MD) simulations to study the monomeric structure of the apoC-II(60–70) peptide

* Corresponding author. Tel.: +61 3 9925 1974; fax: +61 3 9925 3747.
E-mail address: andrew.hung@rmit.edu.au (A. Hung).

1093-3263/$ – see front matter © 2010 Elsevier Inc. All rights reserved.
doi:10.1016/j.jmgm.2010.11.001

under experimentally known fibril-enhancing and fibril-inhibiting conditions [9]. To enhance sampling of all-atom MD, we have applied umbrella sampling methods to calculate the free energy of dimerisation of this peptide under lipid-rich and lipid-depleted conditions [17]. Based on these simulations, it was hypothesised that lipids inhibit fibrillisation by stabilising oligomers which are incapable of propagating fibril formation. This hypothesis was consistent with results from subsequent ultracentrifugation experiments [17], which confirmed the presence of oligomers in mixed lipid-peptide solutions. Other advanced methods, such as replica-exchange MD [18], have also been applied to study aggregation of amyloidogenic peptides [19,20]. A more recent method of enhanced sampling for studying protein dynamics and aggregation is metadynamics, which enables exploration of conformational space along pre-defined reaction coordinates [21,22].

Although advanced methods in conformational sampling have enabled the study of the formation of oligomers at atomistic resolution, aggregation phenomena at biologically relevant length and time-scales are still computationally intractable. To bridge the gap between the short time and length-scales of atomistic molecular simulations and experimental-scale phenomena, mesoscale coarse-grained (CG) molecular models have been developed, enabling faster computation albeit at the cost of atomistic detail. CG models have been applied specifically for the study of amyloid fibril formation. A CG forcefield, together with the "activation–relaxation technique" sampling method was applied by Wei et al. [23] to study fibrillation of KFFE. Similarly, Urbanc et al. [24] used a 4-colour bead model, in conjunction with discrete MD (DMD), to examine Aβ oligomerisation. Models capable of describing mature fibril formation include those of Pellarin and Caflisch [25], who recently developed a simple, two-state model capable of imitating fibril-like peptide ordering from an initial random peptide dispersion; and Bellesia and Shea [26], whose chiral model reproduces fibril ribbon twist.

CG methods have also been applied to the study of biological lipids and their interactions with proteins and peptides. One of the most demonstrably successful CG forcefields is MARTINI [27,28], which has been employed to study peptide–micelle interactions, peptide toxin self-assembly and membrane insertion [29,30], and membrane protein–lipid self-assembly [31,32]; more examples are described in [33]. In this model, significant computational speed-up is possible due to a number of factors. Firstly, the coarse-graining scheme produces a reduction in the total number of particles, and therefore a significant reduction in the number of non-bonded interactions, in the simulation system. Secondly, larger simulation timesteps may be used as a result of the removal of fast degrees of freedom such as individual (i.e. atomic-level) bond length/angle vibrations and torsion angle rotations, the latter in cases where four or more atoms are combined and treated as a single interaction site. Furthermore, there is a "smoothing" of the potential as a result of combining several atoms into single sites, which in turn produces smoother free energy landscapes which are more easily explored by unbiased simulation dynamics (in contrast to rugged, atomistic landscapes, which contain multitudes of local energy minima). Since the MARTINI forcefield was parameterised specifically for interactions between amino acids and lipid bilayers, it is a potentially powerful approach to study the interactions between lipids and peptides, such as apoC-II(60–70), which may lend further important insights into the mechanisms by which lipids inhibit fibrillisation.

In the present work, we have applied the MARTINI forcefield to study the aggregation of multiple copies of the apoC-II(60–70) peptide, the self-assembly of short-chain phosphatidylcholine (PC) lipids (experimentally demonstrated to inhibit fibrillisation), as well as the self-assembly of a combined peptide–lipid mixture, in order to obtain qualitative insights into the fibril-inhibition mechanisms of the lipid. These CG simulation results provide experimentally verifiable hypotheses regarding the structures of the non-fibrillar peptide–micelle complexes. We compare the results obtained by the above-mentioned CG methods with our previous atomistic simulations and experimental studies [8,9,17].

2. Methods

2.1. MARTINI molecular models and parameters

We have employed the MARTINI forcefield [27,28] to study the aggregation behaviour of the apoC-II(60–70) peptide in pure water and in the presence of short-chain PC-like lipids. This forcefield has been successfully applied in numerous studies of peptide and protein–lipid interactions [33], C60–lipid interactions [34], and lipid phase separation [35]. It uses a four-to-one (4–1) atom-site mapping, in which typically four (4) heavy atoms (i.e. non-hydrogen atoms) are represented by a single interaction site, reducing the granularity of representation of the molecule. The model takes into account four main types of interaction sites: polar (P), nonpolar (N), apolar (C), and charged (Q). For particles of type N and Q, four subtypes (0, d, a, and da) are further distinguished. Subtype 0 applies to groups in which no hydrogen-bonding capabilities exist, d and a are for groups that could act as a hydrogen-bond donor or acceptor, respectively, and da is for groups with both donor and acceptor options. All non-bonded particles interact via a Lennard–Jones (LJ) potential. In addition to the LJ interaction, charged groups (type Q) interact via the electrostatic Coulombic potential. The particle types for most amino acids were determined by comparison between simulation results and experimental measurements of the water-oil partition coefficients of the amino acid analogues. Details of the assignment of particle types and coarse-grained force field parameters for amino acids can be found in Monticelli et al. [28]

We have constructed models of the apoC-II(60–70) peptide and PC lipid molecules following the methodology prescribed by Monticelli et al. [28]. The amino acid sequence for the peptide is MSTYTGIFTDQ. For the peptide, each amino acid is represented by a single backbone bead (shown as green spheres in Fig. 1A) harmonically bonded to sidechain beads (yellow spheres, Fig. 1A). Except for glycine, all residues consist of at least one sidechain bead. Tyrosine and phenylalanine sidechains are composed of three beads to model their molecular planarity. We assign all bonded and non-bonded interaction parameters for the amino acids according to Monticelli et al. [28]. The peptide is composed of a series of CG residues harmonically linked via the backbone beads. Backbone bonded parameters are dependent on the pre-defined secondary structure of the residues (helix, strand or coil). Thus, in the current implementation of MARTINI, significant backbone structural transitions generally do not take place. In the current work, we assign backbone bonded parameters consistent with random coil for all residues of the peptide. This choice is justified, given that the peptide exhibits a significant bias (>60% of the time from a 600 ns trajectory) towards random coil conformations in atomistic MD simulations [9].

For the DHPC lipid, we have used all bonded and non-bonded parameters as provided in the MARTINI forcefield [27,28]. Specifically, we model each of the two hydrophobic tails with two C-type beads; the choline group modelled as a positively charged Q_0-type bead; the phosphate group as a negatively-charged Q_a bead; and the glycerol backbone as two polar P-type beads. The model is shown in Fig. 1B. This model represents lipids of aliphatic carbon chain lengths between 8 and 11. Although lipid chain length is ambiguous in a CG model, this is not a significant problem in our current study, as PC lipids of lengths from C4 to C12 have been

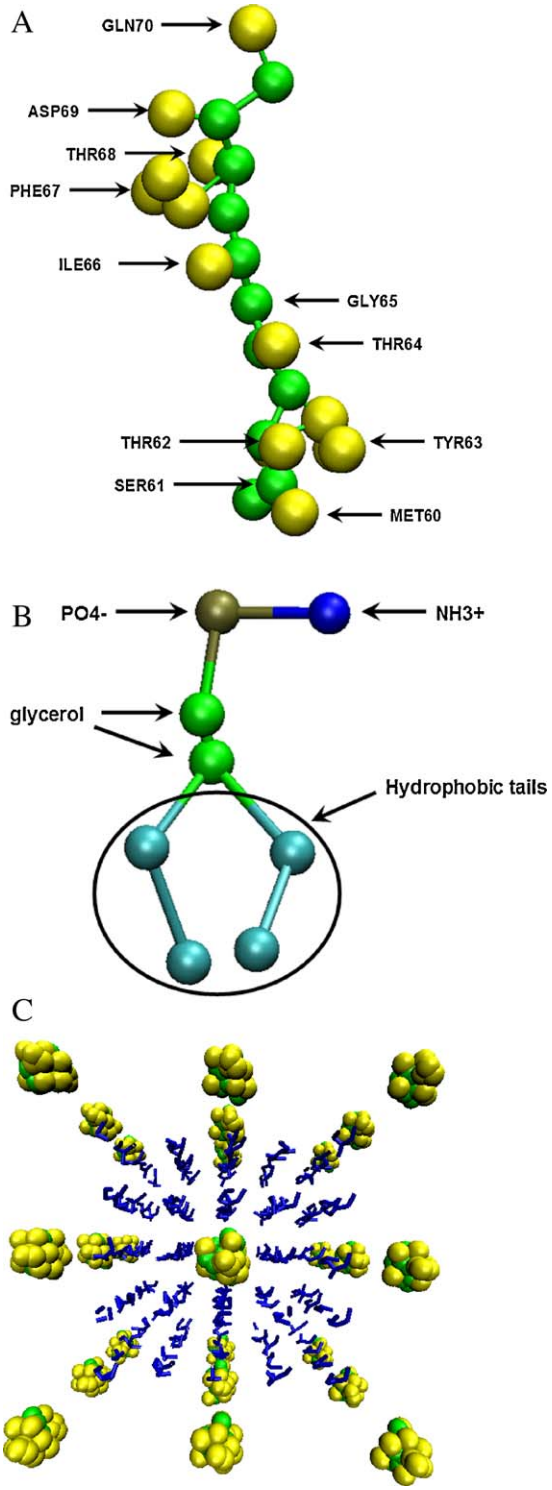

Fig. 1. MARTINI model representations of (A) the apoC-II(60–70) peptide, for which green spheres represent peptide backbone beads, and yellow spheres represent sidechain beads; (B) DHPC lipids, with beads labelled according to the chemical functional group for which they represent; and (C) initial configuration of 27PEP–125LIP. Peptides represented as green and yellow spheres, lipids in blue lines. (For interpretation of the references to colour in this figure legend, the reader is referred to the web version of the article.)

experimentally demonstrated to exert similar effects on fibril inhibition [9,17]. All systems simulated are solvated by water molecules represented by single P_{da} beads.

2.2. System set-up and simulation parameters

We have simulated the following systems in which the initial positions of all molecules were arranged in a dispersed configuration: (1) 27 monomers of apoC-II(60–70) in water alone (named 27PEP–0LIP); (2) 27 peptides in water and 125 DHPC (27PEP–125LIP); and (3) 125 DHPC in water (0PEP–125LIP). We have also simulated (4) the self-assembly of peptides in the presence of a pre-formed DHPC micelle (27PEP–125PreLIP); and (5) the self-assembly of DHPC in the presence of a pre-formed peptide aggregate (27PrePEP–125LIP). The initial configurations of 27PEP–0LIP, 27PEP–125LIP and 0PEP–125LIP were set up by placing replicas of the peptide or lipid on evenly spaced lattice points within a rectangular box of 15 nm [3]. Fig. 1C illustrates the initial configuration of 27PEP–125LIP; similar initial configurations were used for 27PEP–0LIP and 0PEP–125LIP simulations. We have also performed replicate simulations in which the initial positions of the peptides and/or lipids are randomised, and find similar results to those reported in this manuscript (data not shown). For 27PEP–125PreLIP, 27 copies of the peptide are placed in random orientations and positions in the simulation cell containing a pre-formed DHPC bicelle (generated from 300 ns simulation of 0PEP–125LIP). For 27Pre-PEP–125LIP, 125 DHPC lipids are placed in random orientations and positions in the simulation cell containing a pre-formed peptide aggregate (generated from 300 ns simulation of 27PEP–0LIP). Details of the DHPC bicelle and peptide aggregate are given in Results and Discussion. We note that, for 27PEP–125PreLIP initially, 6 of the peptides were inserted inside the bicelle. However, they were rapidly ejected from the bicelle interior during the simulation. A similar set-up was used for 27PrePEP–125LIP, with lipids likewise rapidly ejected from the pre-formed peptide aggregate interior. For all systems, the simulation cells employed are large enough to ensure that the separation between a cluster in the simulation cell and that of its mirror image is at least 30 Å. Water beads are used to solvate all simulated systems. Details of the simulation systems are given in Table 1.

All MD simulations were performed using GROMACS version 3.3 [36,37]. MARTINI forcefield simulations were performed under constant particle number, pressure and temperature (NPT) conditions. Temperature coupling was maintained with a Berendsen thermostat [38] with a coupling constant of 40 ps and a reference temperature of 300 K. Electrostatic and van der Waals interactions were smoothly shifted to zero between 0.9 and 1.2 nm. A relative dielectric constant of 20 was used to compensate for the lack of dielectric screening due to the absence of water dipoles in the coarse-grained water model employed [39]. Each system was pressure-coupled isotropically with a Berendsen barostat at 1 bar, a coupling constant of 40 ps and a compressibility value of 1.0×10^{-5} bar^{-1}. The timestep of integration was 30 fs. Analyses were performed using the Gromacs suite of software. Visualisations were performed using VMD [40].

3. Results and discussion

3.1. Lipid-dependent peptide aggregation kinetics

We have examined the aggregation behaviour of (initially dispersed) 27 monomers of the apoC-II(60–70) peptide in pure water (27PEP–0LIP), in the presence of initially dispersed DHPC lipids (27PEP–125LIP), and in the presence of a pre-formed DHPC bicelle (27PEP–125PreLIP). The rate of aggregation and the evolution of

Table 1
Simulation details.

System label	Number of peptides	Number of DHPC	Simulation time (ns)	Number of solvent beads	Initial configuration
27PEP–0LIP	27	0	300	16497 water 27Na$^+$	Dispersed, crystalline
0PEP–125LIP	0	125	300	23758 water	Dispersed, crystalline
27PEP–125LIP	27	125	240	21608 water 27Na$^+$	Dispersed, crystalline
27PEP–125PreLIP	27	125	400	21608 water 27Na$^+$	Peptides randomly dispersed, pre-formed DHPC bicelle
27PrePEP–125LIP	27	125	400	21608 water 27Na$^+$	DHPC randomly dispersed, pre-formed peptide cluster

the peptide–peptide cluster distribution during the course of the simulations may be determined by inspection of the cluster distribution graphs, shown in Fig. 2A–C. These graphs are interpreted as follows: for a given time in the simulation, a blue bar at a given position along the *y*-axis (labelled "Size") indicates the presence of a peptide cluster of that size in the system. For this and all subsequent discussions, a molecule is defined as belonging to a cluster if any of its beads lie within 6 Å of any bead of any other member of the cluster. In this section, we discuss *peptide* clusters only.

For 27PEP–0LIP (Fig. 2A), at 0 ns, the system is composed of a large number of monomers and small clusters (indicated by the blue bars at low values of size). This is consistent with an initially dispersed configuration. The peptides rapidly diffuse and aggregate, forming a distribution of oligmers composed of up to 17 peptides between 10 and 100 ns. At 100–150 ns, only 2 oligomers remain: a dimer and a 25-mer. These two oligomers finally aggregate at ~150 ns to produce a single, elongated cluster composed of all 27 peptides. Thus, in the absence of lipids, aggregation of apoC-II(60–70) is relatively fast, and is complete within 150 ns. This is consistent with experimental observations, which indicate rapid aggregation in pure water [9].

The presence of (initially dispersed) DHPC lipids markedly reduces the peptide aggregation rate, however. Fig. 2B shows the peptide cluster distribution graph for simulation 27PEP–125LIP. At 0 ns, the peptides are separated, with no peptide oligomers present. Thereafter, peptide cluster growth is slower than that of 27PEP–0LIP, with the formation of oligomers no larger than pentamers by 120 ns. During this phase of the simulation, the system consists of relatively small micelles with surface-bound small peptide oligomers. This portion of the trajectory is representative of a peptide–lipid mixture in which the lipid concentration is not too far above the CMC, and the results are in qualitative agreement with experiments, which demonstrated the aggregation–inhibition effects of lipids as well as the formation of oligomers in solutions containing mixtures of apoC-II(60–70) and DHPC lipids; they are also in qualitative agreement with our previous umbrella sampling simulations, in which we showed that lipids can stabilize peptide dimers [17]. The reduction in aggregation kinetics (compared to that of a lipid-free environment) may be due to the strong association of peptide oligomers with the lipid micelles; the overall charge of each peptide–lipid micelle complex is negative (owing to Asp), thus imparting an additional degree of mutual

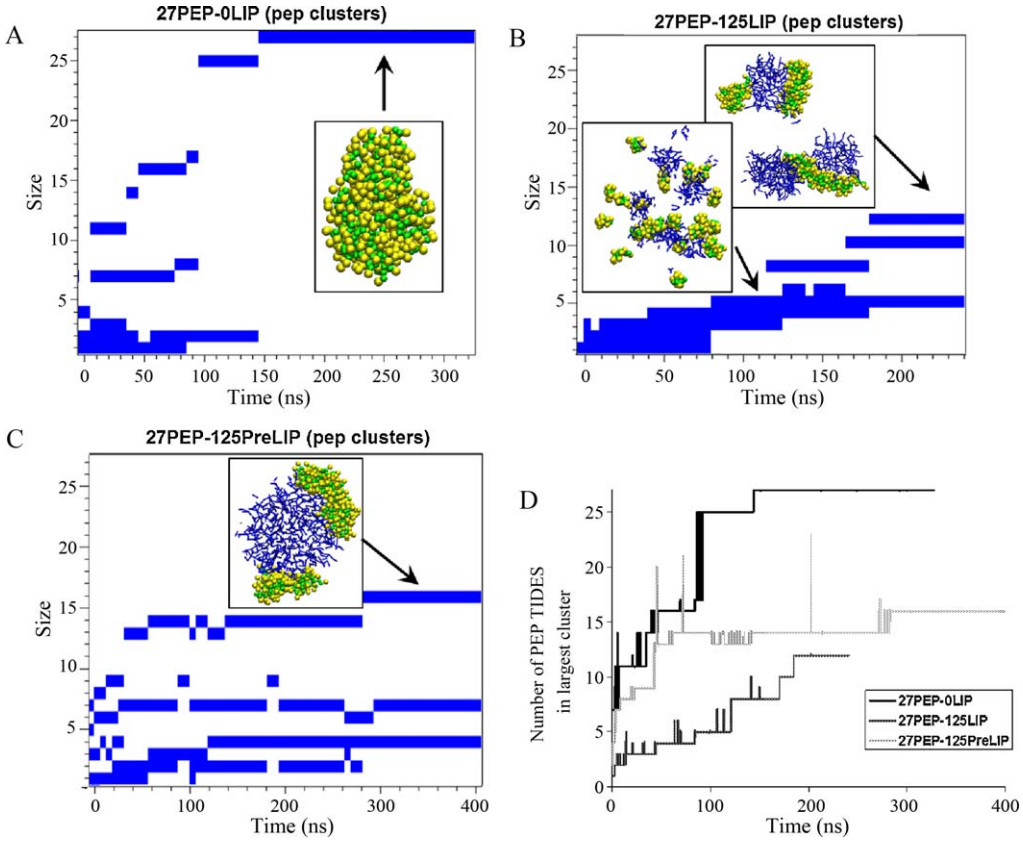

Fig. 2. Peptide–peptide cluster size distribution with respect to simulation time for (A) 27PEP–0LIP; (B) 27PEP–125LIP; and (C) 27PEP–125PreLIP. Simulation snapshots illustrating the structures of the aggregates formed are inset. Peptides are shown as green and yellow spheres, lipids as blue lines. (D) Graph of the number of peptides in the largest peptide cluster with respect to time for 27PEP–0LIP (black line), 27PEP–125LIP (dark grey) and 27PEP–125PreLIP (light grey). (For interpretation of the references to colour in this figure legend, the reader is referred to the web version of the article.)

repulsion between the micelles. The repulsive electrostatic interaction results in the existence of a free energy barrier which must first be overcome before combination of existing complexes can take place. Further aggregation between the peptide–lipid micellar complexes results in the formation of a heptamer, bound to a micelle composed of ~50 lipids, which persists from 120 to 160 ns. Finally, three oligomers are formed, composed of 5, 10 and 12 peptides each. Thus, the presence of DHPC lipids prevents the complete aggregation of the peptides into a single, large cluster within the simulated timeframe. Instead, separate peptide clusters are formed. The largest one is bound to 2 lipid micelles (Fig. 2B, lower right hand graphical inset), while the other two peptide clusters are both bound to 1 lipid micelle (Fig. 2B, upper right hand inset).

The presence of a pre-formed DHPC lipid bicelle (i.e. a large DHPC cluster composed of 125 lipids) also prevents the peptides from complete aggregation within the simulated timeframe. Fig. 2C shows the cluster distribution graph for 27PEP–125PreLIP. As with the two simulations discussed above, the initial configuration contains a large number of small-sized peptide clusters. The small clusters aggregate rapidly, forming a distribution composed of clusters of sizes 14, 7 and 4 by ~100 ns. It is apparent that the peptide aggregation kinetics is not substantially influenced by the presence of the bicelle, as much of the initial aggregation events take place outside the bicelle (i.e. in an environment similar to pure water). The peptides firstly form clusters with each other, and then subsequently adsorb onto the surface of the bicelle as oligomers. Further aggregation does not occur until ~300 ns, with the final formation of three clusters, the largest one composed of 16 peptides. All three clusters are bound to separate regions on the single (pre-formed) lipid bicelle, as shown in the graphical inset of Fig. 2C.

The relative rates of peptide aggregation for the three simulations discussed above is summarised in Fig. 2D, which shows the size (in terms of number of constituent peptides) of the *largest* peptide cluster in each system with respect to time. Consistent with the cluster distribution graphs, the largest cluster size plots indicate that aggregation is most rapid in the absence of lipids and proceeds to completion with incorporation of all 27 monomers in the system (27PEP–0LIP, black line). In the presence of a pre-formed bicelle (27PEP–125PreLIP, light grey line), the rate of aggregation (determined by the line gradient) is initially comparable to that of the peptides in pure water up to ~100 ns. However, aggregation does not proceed further, as the peptide clusters are tightly bound to the bicelle surface. In the presence of an initially dispersed solution of lipids (27PEP–125LIP), the peptide aggregation kinetics is substantially slower throughout (with a lower line gradient), and furthermore does not proceed to completion. Overall, our simulations suggest that lipids may prevent the aggregation of apoC-II(60–70) by strongly binding them in peptide–lipid micelle-like complexes, effectively "trapping" small and medium-sized peptide oligomers and preventing them from undergoing further aggregation to form larger oligomers.

3.2. Peptide aggregation mechanism and inhibition by lipids

In order to elucidate the principal driving forces for the aggregation of apoC-II(60–70), we have examined the number of inter-peptide contacts for a number of selected residues with respect to simulation time. These are shown in Fig. 3A, which indicates the total number of residue-to-residue contacts between different peptides for the 27PEP–0LIP simulation (for example, the curve for "Phe" (light grey) indicates the number of Phe-to-Phe contacts between different peptides). The residues chosen are those that formed the most number of contacts during the simulation; residues that do not show substantial contacts (being <10 contacts throughout the simulation) are excluded. Inspection of the figure shows that the most rapidly formed inter-peptide contacts are those between Phe residues, which show substantial growth in contact numbers from 0 to 70 ns (grey line). Overall, Phe-to-Phe contacts are also the highest out of all of the residues examined. After ~50 ns, inter-peptide contacts between Tyr residues begin to increase in number (light green line), becoming another dominant interaction throughout the simulation. Thr and Ile contacts also begin to increase after ~50 ns. These results suggest the following interaction mechanism: initially, Phe-to-Phe interactions constitute the first contacts between the peptides as they initially begin to form oligomers, as illustrated by the graphical inset in Fig. 3A. This is followed by the formation of Tyr contacts, and other interactions via Thr and Ile. These observations suggest that the primary driving force for peptide aggregation is via hydrophobic interactions, mediated through aromatic sidechains. The persistence of hydrophobic contacts throughout the trajectory indicates that, in addition to facilitating initial contact, aromatic residues also play an important role in maintaining aggregate stability. This mechanism highlights the important role of aromatic residues in oligomer formation as well as growth, consistent with our previous findings from atomistic MD simulations of apoCII(60–70) peptide monomers [9], in which factors such as pH and M60 oxidation were found to influence the relative positions of the aromatic sidechains. The importance of aromatic residues is also highlighted by Flock et al. [41], in which the contributions of Phe to the aggregation of small amyloidogenic peptides such as FF and NFGAIL were studied.

We note that another possible driving force for inter-peptide association is electrostatic interactions. For apoC-II(60–70), the only electrostatic interactions present are those between peptide termini, and between Asp sidechains and N-termini. To determine whether electrostatic attraction plays a role in promoting peptide aggregation, we have examined both types of inter-peptide contacts (namely, inter-peptide N-termini contacts with C-termini (blue line), and inter-peptide Asp contacts with N-termini (red line)). We find that although some electrostatic attraction contacts are formed and maintained throughout the trajectory, the numbers of contacts are far below that between Phe and Tyr. This indicates that hydrophobic, rather than electrostatic, attraction is the chief determinant of apoC-II(60–70) aggregation.

Given the importance of Phe-to-Phe contacts in peptide aggregation discussed above, we have examined the effects of the presence of lipids on these interactions. Time series plots of inter-peptide Phe contacts (grey line), as well as between Phe and the hydrophobic tails of DHPC (black line), for the 27PEP–125LIP simulation is shown in Fig. 3B. Inspection of the plots reveals that there is an initial rapid rise in the number of contacts between Phe and lipid tails between 0 and 50 ns. Concurrently, the number of inter-peptide contacts between Phe residues is markedly lower, and does not exhibit the rapid increase seen in the lipid-free 27PEP–0LIP simulation (Fig. 3A). These results suggest that Phe residues tend to bind to lipid tails, in preference to other Phe residues. The aggregates that are formed thus consist of peptide oligomers whose Phe sidechains are partially buried into the lipid micelles to which they are bound (see graphical inset). This result suggests that one mechanism by which lipids cause reduced aggregation kinetics of peptide is by competitive binding with the Phe sidechains of the peptide, reducing the probability of inter-peptide Phe contacts, which is a major driving force for aggregation. The persistence of Phe-tail contacts throughout the trajectory also suggests that the peptide aggregates are stabilised by hydrophobic sidechain burial into micelles, discouraging further aggregation of the peptide oligomers into larger clusters. We also note that, as expected, charged Asp residues do not interact strongly with the hydrophobic interior of DHPC micelles (red line).

3.3. Peptide aggregate structure

We examine the structure of the final apoC-II(60–70) peptide aggregate in water and in the presence of lipids. We note that the current CG model is unlikely to predict the formation of mature fibrils. This is due to the lack of atomistic detail of the peptide backbone, which is a necessary component for accurate modelling of the inter-backbone hydrogen bonding present in amyloid fibrils. Nevertheless, the disordered aggregate identified from CG simulations enables the study of the *intermediate* clusters which are formed as part of fibrillogenic pathways. Such clusters are stabilised largely by sidechain–sidechain interactions (especially hydrophobic interactions) and are formed prior to the formation of inter-backbone H-bonds. This is similar in principle to the approach of employing (short timescale) atomistic simulations to study aggregation of amyloid peptide clusters, which enables elucidation of pre-fibrillar disordered aggregates [41].

The shape and dimensions of the cluster may be quantified by calculating the lengths of the three principal axes. Namely, the first principal axis (PA1) measures its size along the axis which points along its longest direction (i.e. "length"). The second and third principal axes (PA2 and PA3) measure its size along its second longest and third longest directions, respectively ("width" and "depth"). Bar charts indicating the sizes of the peptide cluster along the three principals for 27PEP–0LIP, 27PEP–125LIP and 27PEP–125PreLIP are shown in Fig. 4. Each of the PA measurements was taken as an average over the final 50 ns of simulations, with standard deviations shown as error bars. For the 27PEP–0LIP simulation, the structure of the final peptide cluster is linear and elongated. This is quantified by a long PA1; and similar values of PA2 and PA3, consistent with a structure that is extended, but resembles an approximate circle when viewed directly along PA1. The structure is shown from two different perspectives in the first 2 graphical insets of Fig. 4. The overall morphology is reminiscent of the structures of self-assembled small fibril-forming peptides as deter-

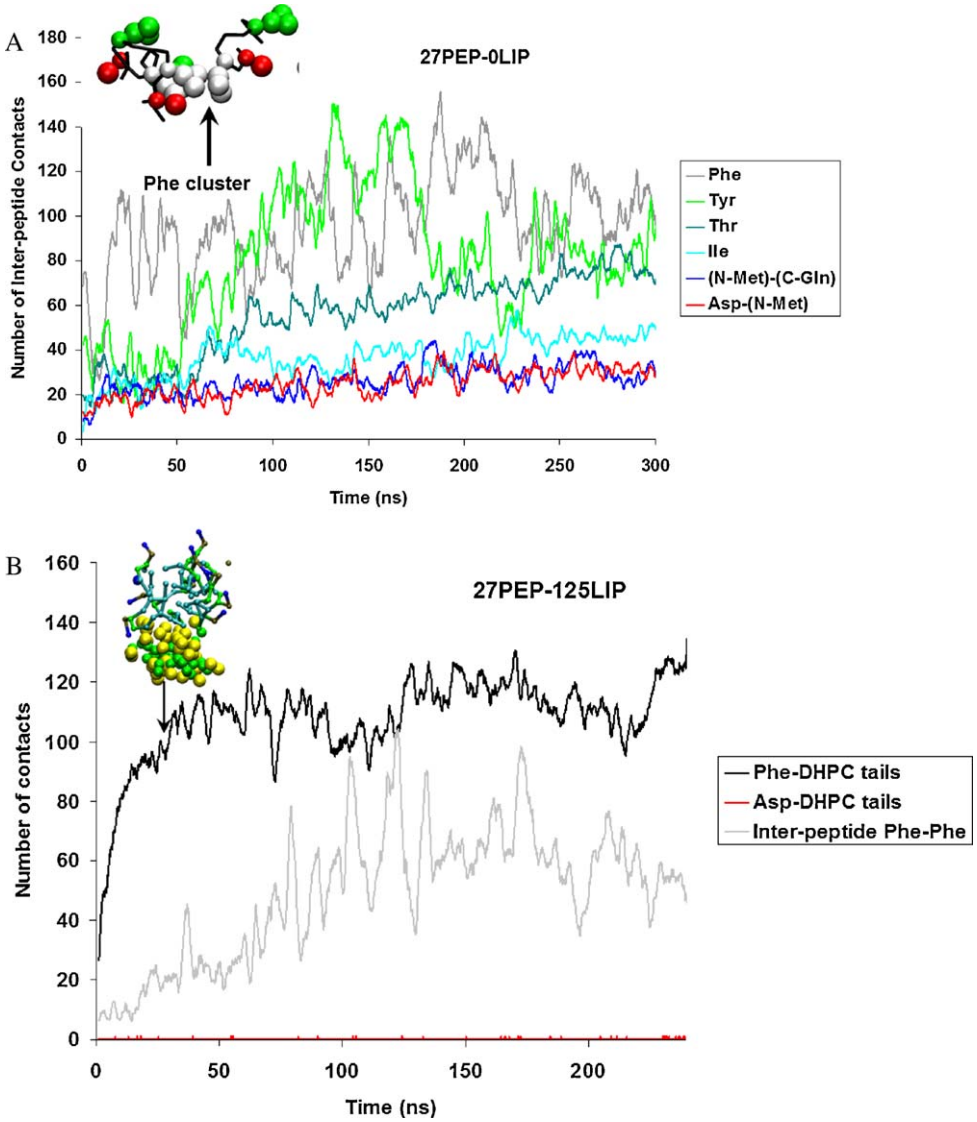

Fig. 3. (A) Graph of the number of inter-peptide residue-to-residue contacts with respect to time for Phe (grey), Tyr (light green), Thr (dark green), and Ile (light blue), for the 27PEP–0LIP simulation. Also shown are plots of the number of inter-peptide contacts between N- and C-termini (dark blue), and number of inter-peptide contacts between Asp and N-termini (red). Snapshot illustrating the initial contact between two peptides via Phe sidechains (shown as light grey spheres) is inset. Tyr and Asp are shown as green and red spheres, respectively. (B) Number of contacts between Phe and DHPC hydrophobic tails (black), between Asp and DHPC tails (red), and Phe-to-Phe contacts between peptides (light grey) for the 27PEP–125LIP simulation. Inset shows a snapshot of peptide oligomer forming contacts with lipid tails (cyan spheres and rods). Curves are smoothed by averaging over 2 ns.

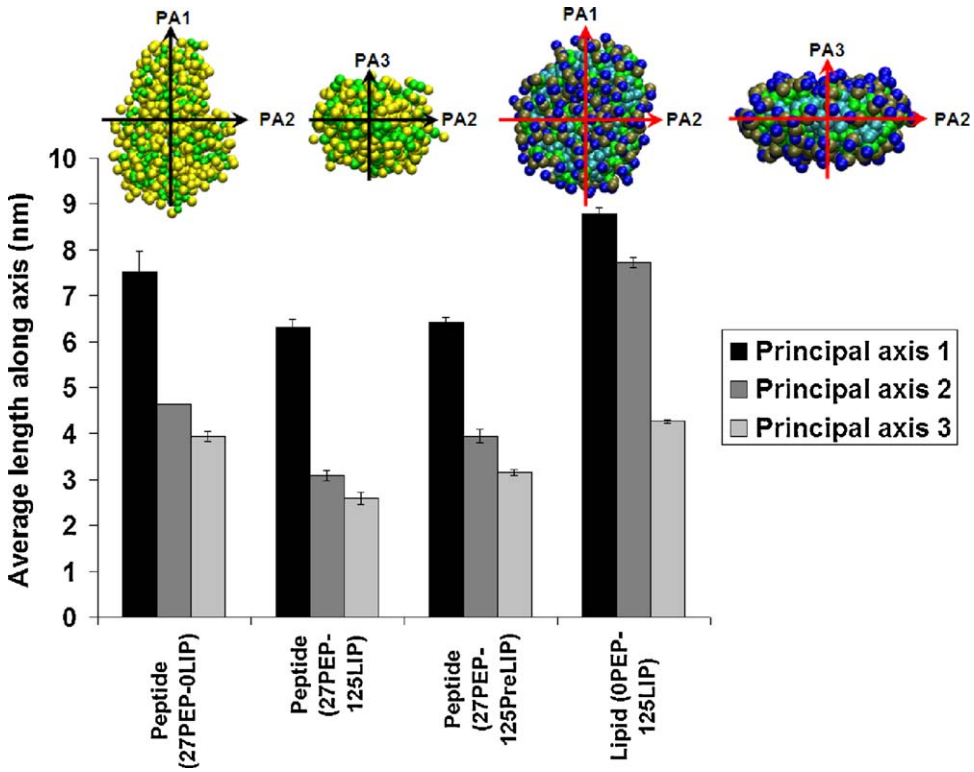

Fig. 4. Bar chart showing the lengths of the three principal axes of the peptide aggregates in simulations 27PEP–0LIP, 27PEP–125LIP and 27PEP–125PreLIP; and of the lipid bicelle in simulation 0PEP–125LIP. Lengths are averaged over the final 50 ns of simulations, with standard deviations shown as error bars. Snapshots of the aggregates with approximate lengths of the principal axes (PA1–3) indicated are inset.

mined by atomistic MD simulations [41]. It has also been proposed that MD simulations of small peptide aggregates can be used as a predictive measure of the amyloidogenic propensity of a peptide, because fibrillogenic peptides form disordered aggregates with elongated morphologies, whereas non-fibrillogenic peptides form approximately spherical disordered aggregates with no apparent directional bias. In the case of apoC-II(60–70), our current CG simulation indicates the formation of a clearly elongated cluster, and thus suggests (correctly) that this peptide has a high propensity for fibrillogenesis. Our current result is consistent with the hypothesis of Flock et al. [41] put forward on the basis of atomistic MD simulations of small peptide clusters, namely, that the formation of metastable elongated peptide clusters is a pre-requisite for fibril competency.

We note that the 27PEP–0LIP aggregate structure is qualitatively similar to that of 27PEP–125PreLIP (3rd column, Fig. 4); for

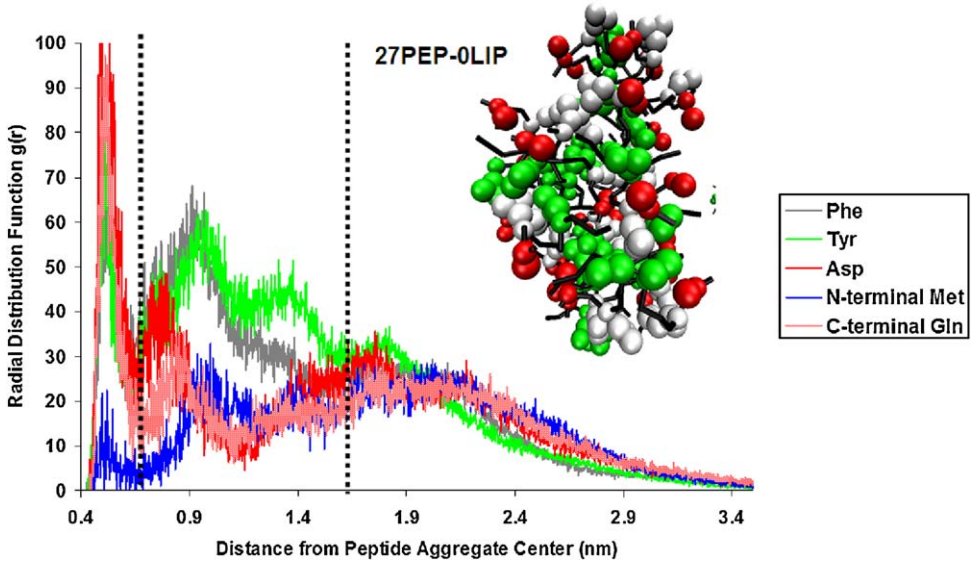

Fig. 5. Radial distribution function $g(r)$ of Phe (grey), Tyr (green), Asp (red), N-termini (blue) and C-termini (pink) with respect to the Met residue of a peptide at the cluster center, for the peptide aggregate in simulation 27PEP–0LIP. Calculated as an average over the final 50 ns. The interior of the cluster is between ~0.7 and 1.7 nm, demarcated by dotted lines. Graphic illustrating the cluster structure is inset, with the same colour coding for the residues as the $g(r)$ plot. (For interpretation of the references to colour in this figure legend, the reader is referred to the web version of the article.)

the latter, the dimensions of the *largest* peptide aggregate were measured. For both simulations, PA1 is roughly 60% higher than PA2 and PA3. However, there is more marked difference when we consider 27PEP–125LIP (2nd column, Fig. 4), where the length of PA1 is more than 100% higher than PA2 and PA3. This indicates the formation of a more elongated, slender structure. The source of this difference lies in the environment of the peptide cluster. For 27PEP–125PreLIP, the aggregate is simply adsorbed onto the surface of a DHPC bicelle (Fig. 2C, inset); its shape is similar to that of an aggregate formed in water. But for 27PEP–125LIP, the largest peptide cluster is sandwiched between two DHPC micelles (see Fig. 2B, right hand side graphical inset), forming more extensive contacts with lipids. Thus, although both 27PEP–125LIP and 27PEP–125PreLIP contain the same composition of peptides and lipids, it is apparent that the final shape of the peptide aggregate is dependent on its lipid environment. This result highlights the important role of lipids in shaping peptide aggregate morphology. Our simulations suggest that a local environment richer in lipids appears to promote formation of a more elongated peptide aggregate shape. It is of interest to note that full-length apoC-II fibril morphology has been observed to be strongly dependent on lipid concentration [8].

The peptide aggregate predicted by the CG simulations exhibit a number of characteristics of interest. Inspection of the cluster obtained from 27PEP–0LIP shows that, qualitatively, the (charged) aspartates, along with the peptide termini (also charged), are largely excluded from the cluster core, and instead line the exterior of the aggregate. Conversely, the aromatic residues Tyr and Phe reside both inside and also along the exterior of the aggregate. The distribution of these residues throughout the cluster may be further characterised by radial distribution function (RDF, $g(r)$) plots, shown in Fig. 5. The $g(r)$ characterise the relative density of selected residues relative to a reference point. In Fig. 5, the $g(r)$ of Phe (grey), Tyr (green), Asp (red) and the N- (blue) and C-termini (pink) are shown with the reference point selected to be Met residue of a peptide located near the center of the aggregate. The sharp peaks exhibited at low separation from the central peptide (<0.6 nm) are due to residues located on the reference peptide, and may be excluded for the purpose of examining residue distributions throughout the aggregate. Of particular interest is the region between 0.6 and 1.7 nm, which corresponds to the interior of the cluster. Phe and Tyr are particularly dense, indicating the prevalence of aromatic residues in the aggregate core. This further reinforces the notion that aromatic residues play a vital role in stabilising peptide clusters. In contrast, charged groups such as Asp and the termini exhibit relatively low $g(r)$, indicative of depleted density in the core regions. These groups, however, are more prevalent in the exterior of the cluster (>1.6 nm). We note that, being partially polar, Tyr is also highly represented on the cluster surface. Thus, the apparently disordered peptide aggregate exhibits a distinct bias towards hydrophobic residues in its interior, while hydrophilic and charged groups are solvent exposed. The largest cluster obtained from 27PEP–125LIP, however, exhibits differences in residue distribution. This is illustrated in Fig. 6. For this cluster, the Phe groups interact with (and partly insert into) the two DHPC micelles on either side of the cluster, while the Asp residues are located further away from the micelles (see Fig. 3B). The attraction of Phe, and repulsion of Asp, towards the micelles results in an approximate linear alignment of the Phe and Asp.

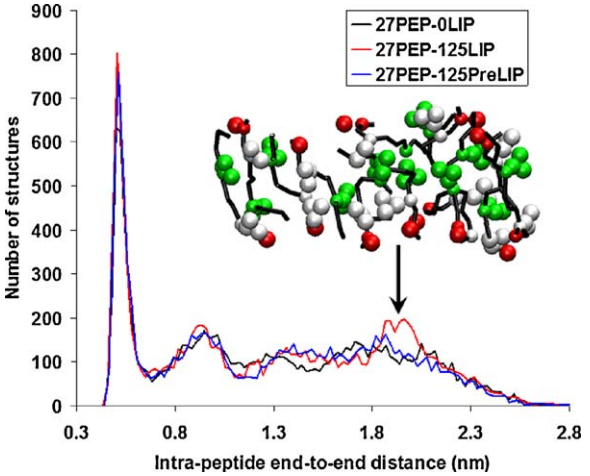

Fig. 7. Histogram of peptide end-to-end distances for simulations 27PEP–0LIP (black line), 27PEP–125LIP (red), and 27PEP–125PreLIP (blue). The *y*-axis indicates counts of the number of peptide structures with a given end-to-end length over the final 50 ns of the simulations. A segment of the peptide aggregate from 27PEP–125LIP is inset, showing alignment of extended peptides with colour coding identical to Fig. 6. (For interpretation of the references to colour in this figure legend, the reader is referred to the web version of the article.)

Additionally, despite the overall disorder of the cluster, some segments of it are composed of ordered stacking involving extended peptides, which resemble those in fibrillar aggregates. Fig. 7 presents histograms of the end-to-end distances of individual peptides within the largest clusters formed in the 27PEP–0LIP (black line), 27PEP–125LIP (red) and 27PEP–125PreLIP (blue) simulations. All of the aggregates exhibit a distinct sharp peak at ~0.5 nm, indicating that peptides in these clusters primarily adopt hairpin conformations in which the (intra-peptide) termini are

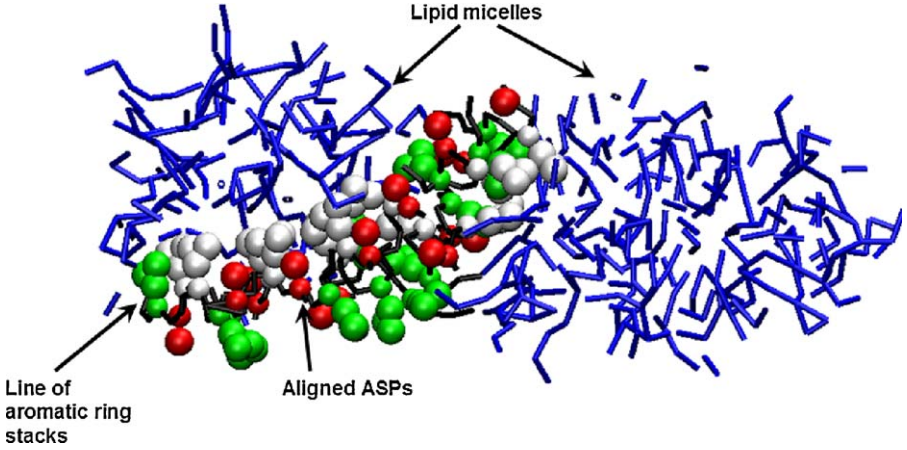

Fig. 6. Illustration of the structure of one of the "macroclusters" at 200 ns from simulation 27PEP–125LIP. Phe in grey spheres, Asp in red, and Tyr in green. Peptide backbones shown as black lines. Lipids are shown as blue lines. (For interpretation of the references to colour in this figure legend, the reader is referred to the web version of the article.)

close to each other. However, a substantial proportion of the peptides adopt extended conformations, indicated by histogram peaks at ~1.8 nm. Inspection of the aggregate structures indicate that such extended peptides are in close proximity to each other, and are aligned with each other in an anti-parallel fashion, in qualitative agreement with our previous simulations which show that apoC-II(60–70) anti-parallel dimers are stable and have high dissociation free energy [17]. In particular, the largest cluster from simulation 27PEP–125LIP contains more extended peptides (illustrated by the graphical inset in Fig. 7, which also illustrates the extensive aromatic ring stacking interactions present throughout the cluster). This may be related to its overall greater elongation as a result of higher contacts with DHPC micelles (discussed above, also see Fig. 4, 2nd column) compared to aggregates obtained from the other simulations.

Overall, despite the current inability of the CG model to predict fibril formation owing to the lack of sufficient peptide backbone detail, our simulation shows that the peptide's physical properties encoded in its amino acid sequence enforce a degree of order upon the aggregates it forms, resulting in the formation of a disordered (but not random) aggregate. Such aggregates exhibit strong directional bias and may serve as precursors to elongated fibrils. These combined factors place strong free energy constraints on the structure of the resultant disordered peptide aggregate, in direct analogy with the fact that the sequence of amino acids in a protein dictates its three-dimensional fold.

3.4. Lipid aggregation and the influence of peptides

In addition to the effects of lipids on apoC-II(60–70) aggregation, it is also of interest to examine the influence of the peptide on lipid self-assembly, in light of experimental studies which point towards small oligomers of amyloidogenic peptides as cytotoxic species, whose effects may be exerted via disruption of membrane structures [42]. We have therefore examined the self-assembly and phase behaviour of the DHPC model in the absence and presence of apoC-II(60–70) peptides.

We characterise the aggregation kinetics of DHPC lipids by examining the lipid–lipid cluster distributions with respect to time, as shown in Fig. 8A–C. In these plots, we consider *lipid* clusters only. For the 0PEP–125LIP simulation (Fig. 8A), the lipids firstly form a suspension of small micelles between 0 and 20 ns (see left hand side

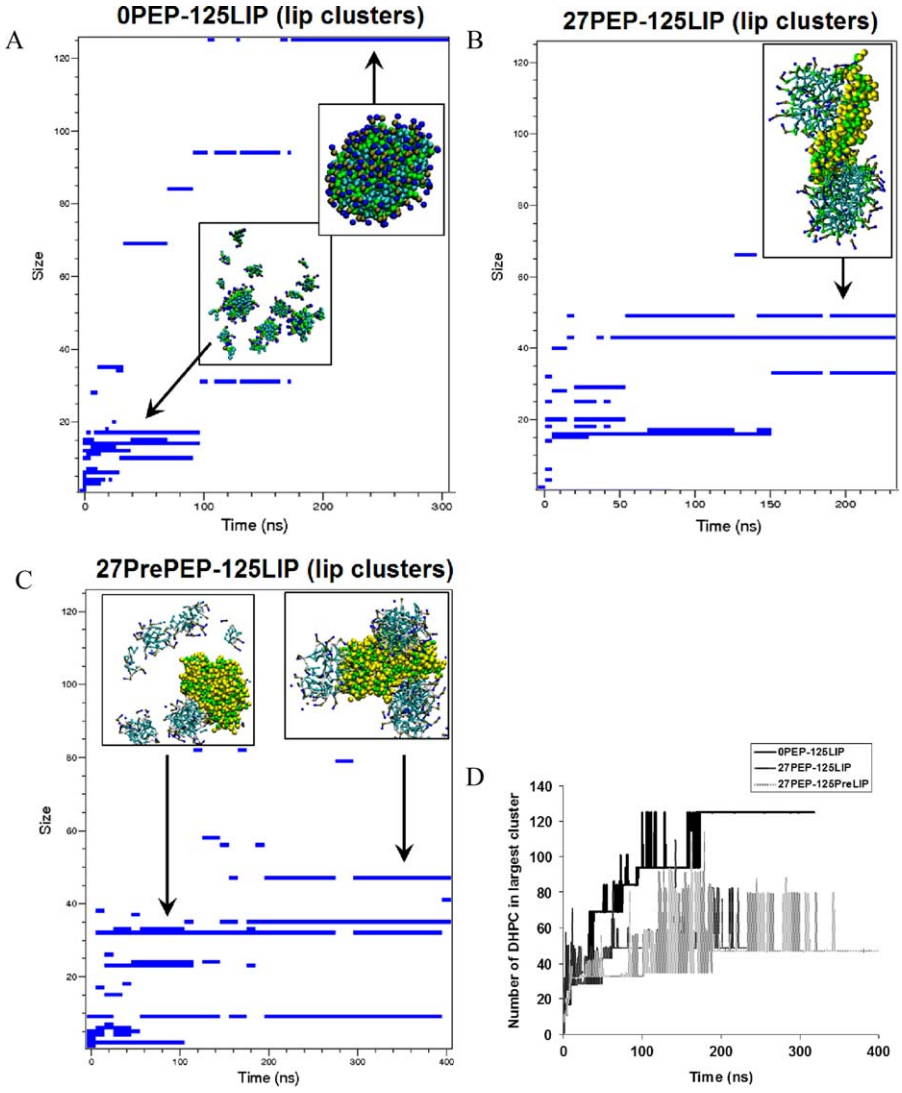

Fig. 8. DHPC lipid–lipid cluster size distribution with respect to simulation time for (A) 0PEP–125LIP; (B) 27PEP–125LIP; and (C) 27PrePEP–125LIP. Simulation snapshots illustrating the structures of the aggregates formed are inset. Peptides are shown as green and yellow spheres. DHPC colour coded as follows: hydrophobic tails (cyan rods), choline (blue spheres), phosphate (bronze spheres), and glycerol (green spheres). (D) Graph of the number of DHPC lipids in the largest lipid cluster with respect to time for 0PEP–125LIP (black line), 27PEP–125LIP (dark grey) and 27PrePEP–125LIP (light grey). (For interpretation of the references to colour in this figure legend, the reader is referred to the web version of the article.)

graphical inset). Small oligomeric (dimers and trimers) complexes rapidly form between 0 and 10 ns due to strong hydrophobic interactions between the carbon tails of adjacent lipids. In this portion of the trajectory, lipid cluster growth is dominated by the diffusion and subsequent addition of single lipids or small oligomers; thus micelle formation in this phase of the self-assembly process exhibits relatively fast kinetics. This is subsequently followed by the formation of larger ("intermediate size") micelles between 20 and 180 ns. This stage involves diffusion and combination of larger aggregates, which is a slower process, manifested in the slower formation of new larger lipid aggregates beyond 20 ns (Fig. 8A). Between 95 and 100 ns, several intermediate-size micelles undergo further rapid combination to form two large micelles, one composed of ~94 lipids and the other the remaining 31 lipids. Finally, a bicelle-like structure composed of all 125 lipids in the system is formed and is sustained throughout the rest of the simulation (right hand side inset). The bicelle resembles a disc, and its dimensions are quantified in Fig. 4 (4th column). The first two principal axes (PA1 and PA2) are large and similar, indicating a roughly circular shape along the PA1–PA2 plane; while PA3 is much smaller, indicative of a slender thickness. The structure is shown from two different perspectives in the last 2 graphical insets of Fig. 4.

The simulation thus suggests that, at this concentration (~70 mM), the lipid undergoes stepwise phase conversions from small micelles, through to progressively larger micelles, and finally to a bilayer-like structure, at each stage growing by way of combinations of existing micelles. The multiple phases exhibited in this simulation system enable a study of the effects of different lipid phases on peptide aggregation; specifically, peptide binding to relatively small micelles, as well as peptide binding to larger, bilayer-like aggregates (discussed in *Lipid-Dependent Peptide Aggregation Kinetics* above).

In the presence of peptides (27PEP–125LIP and 27PEP–125PreLIP), the aggregation kinetics for DHPC is markedly reduced. Additionally, the lipids do not aggregate completely, and do not form a single bicelle structure composed of all 125 lipids. This can be determined by inspection of Fig. 8B and C. In both of these simulations, the lipids rapidly form a distribution of intermediate-sized clusters, ranging in size from 15 to 50 lipids, within 100 ns. However, this distribution becomes stabilised and persists for the remainder of the trajectories. The inability of the separate lipid micelles to coalesce and form a single, large bicelle is due to tight binding with the peptide aggregates, as can be seen in the graphical insets in Fig. 8B and C. These results suggest that apoC-II(60–70) aggregates are capable of disrupting the formation of large lipid supramolecular complexes, such as bilayers. The relative rates of lipid aggregation for the simulations discussed above is summarised in Fig. 8D, which shows the size (in terms of number of constituent lipids) of the *largest* lipid cluster in each system with respect to time. Consistent with the cluster distribution graphs, the largest cluster size plots indicate that aggregation kinetics are lower (lower gradients) for 27PEP–125LIP (dark grey line) and 27PEP–125PreLIP (light grey line) compared to 0PEP–125LIP (black line).

Additionally, we note that our 27PEP–125PreLIP simulation suggests that peptide aggregates do not significantly disrupt the pre-formed bicelle (Fig. 2C, inset). In contrast, as discussed above, when the lipids are initially dispersed, the presence of peptides appears to prevent the formation of large lipid aggregates. Therefore, it is possible that while apoC-II(60–70) peptide aggregates may be relatively inert against pre-existing bilayers, they may disrupt the *formation* of bilayers by interfering with lipid self-assembly. This may have implications for explaining the potential cytotoxic mechanisms of amyloid peptide oligomers, which may interfere with membrane reformation associated with routine cellular processes such as endo- and exocytosis.

4. Conclusions

We have employed MD simulations together with the MARTINI coarse-grained forcefield to study the lipid-dependent aggregation of an amyloidogenic peptide, apoC-II(60–70). In water, the peptide rapidly aggregates and forms an elongated cluster with an internal hydrophobic core, while termini and charged residues are solvent exposed. Interactions between aromatic residues promote the initial aggregation and subsequently serve to stabilise the peptide aggregate. In contrast, in the presence of DHPC lipids, peptide aggregation kinetics is markedly reduced, with subsequent formation of a suspension of aggregates composed of smaller peptide oligomers partially inserted into lipid micelles. Both effects are caused by strong interactions between the aromatic residues of the peptide with the lipid hydrophobic tails. Thus, our simulations suggest that lipid-induced aggregate inhibition is partly due to the preferential binding of peptide aromatic sidechains with lipid hydrophobic tails, reducing inter-peptide hydrophobic interactions. In addition, the presence of peptides disrupts the self-assembly of lipids into large oligomeric structures. However, adsorption of peptide aggregates on a pre-formed bicelle does not appreciably affect its structure. It is possible that while apoC-II(60–70) aggregates may be inert against bilayers, they may nevertheless disrupt bilayer formation by interfering with lipid self-assembly, which has possible implications for explaining the cytotoxicity of peptide oligomers.

Acknowledgements

We gratefully acknowledge the National Computational Infrastructure (NCI) and Victorian Partnership for Advanced Computing (VPAC) for provision of computational resources, and the latter for provision of funds through the eResearch grants scheme. We thank our colleagues at RMIT University and the University of Melbourne for helpful discussions.

References

[1] M. Bucciantini, E. Giannoni, F. Chiti, F. Baroni, L. Formigli, J. Zurdo, N. Taddei, G. Ramponi, C.M. Dobson, M. Stefani, Nat. Biotechnol. 416 (2002) 507.
[2] D. Thirumalai, D.K. Klimov, R.I. Dima, Curr. Opin. Struct. Biol. 13 (2003) 146.
[3] M. Stefani, C.M. Dobson, J. Mol. Med. – JMM 81 (2003) 678.
[4] A.-M. Fernandez-Escamilla, F. Rousseau, J. Schymkowitz, L. Serrano, Nat. Biotechnol. 22 (2004) 1302.
[5] A. Kapurniotu, A. Schmauder, K. Tenidis, J. Mol. Biol. 315 (2002) 339.
[6] A. Naito, M. Kamihira, R. Inoue, H. Saito, Magn. Reson. Chem. 42 (2004) 247.
[7] M.R. Sawaya, S. Sambashivan, R. Nelson, M.I. Ivanova, S.A. Sievers, M.I. Apostol, M.J. Thompson, M. Balbirnie, J.J.W. Wiltzius, H.T. McFarlane, A.O. Madsen, C. Riekel, D. Eisenberg, Nature 447 (2007) 453.
[8] M.D.W. Griffin, M.L.Y. Mok, L.M. Wilson, C.L.L. Pham, L.J. Waddington, M.A. Perugini, G.J. Howlett, J. Mol. Biol. 375 (2008) 240.
[9] A. Hung, M.D.W. Griffin, G.J. Howlett, I. Yarovsky, Eur. Biophys. J. Biophys. Lett. 38 (2008) 99.
[10] S.D. Maleknia, N. Reixach, J.N. Buxbaum, FEBS J. 273 (2006) 5400.
[11] A.L. Bergstrom, J. Chabry, L. Bastholm, P.M.H. Heegaard, BBA – Proteins Proteomics 1774 (2007) 1118.
[12] T. Bandiera, J. Lansen, C. Post, M. Varasi, Curr. Med. Chem. 4 (1997) 159.
[13] S. Moore, J. Askew, G. Gibson, A. Aborgrein, T. Huckerby, O. El-Agnaf, D. Allsop, D. Leung, R. Breslow, Neurobiol. Aging 23 (2002) S105.
[14] B.M. Austen, K.E. Paleologou, S.A.E. Ali, M.M. Qureshi, D. Allsop, O.M.A. El-Agnaf, Biochemistry 47 (2008) 1984.
[15] E.S. Legge, H. Treutlein, G.J. Howlett, I. Yarovsky, Biophys. Chem. 130 (2007) 102.
[16] F.S. Legge, K.J. Binger, M.D.W. Griffin, G.J. Howlett, D. Scanlon, H. Treutlein, I. Yarovsky, J. Phys. Chem. B 113 (2009) 14006.
[17] A. Hung, M.D.W. Griffin, G.J. Howlett, I. Yarovsky, J. Phys. Chem. B 113 (2009) 9447.
[18] Y. Sugita, Y. Okamoto, Chem. Phys. Lett. 314 (1999) 141.
[19] B. Strodel, C.S. Whittleston, D.J. Wales, JACS 129 (2007) 16005.
[20] A. Baumketner, J.-E. Shea, J. Mol. Biol. 366 (2007) 275.
[21] A. Laio, M. Parrinello, PNAS 99 (2002) 12562.
[22] N. Todorova, F. Marinelli, S. Piana, I. Yarovsky, J. Phys. Chem. B 113 (2009) 3556.
[23] G.H. Wei, N. Mousseau, P. Derreumaux, Biophys. J 87 (2004) 364.

[24] B. Urbanc, L. Cruz, S. Yun, S.V. Buldyrev, G. Bitan, D.B. Teplow, H.E. Stanley, PNAS 101 (2004) 17345.
[25] R. Pellarin, A. Caflisch, J. Mol. Biol. 360 (2006) 882.
[26] G. Bellesia, J.-E. Shea, J. Chem. Phys. 126 (2007) 245104.
[27] S.J. Marrink, H.J. Risselada, S. Yefimov, D.P. Tieleman, A.H. de Vries, J. Phys. Chem. B 111 (2007) 7812.
[28] L. Monticelli, S.K. Kandasamy, X. Periole, R.G. Larson, D.P. Tieleman, S.J. Marrink, J. Chem. Theory Comput. 4 (2008) 819.
[29] P.J. Bond, M.S.P. Sansom, JACS 128 (2006) 2697.
[30] P.J. Bond, D.L. Parton, J.F. Clark, M.S.P. Sansom, Biophys. J. 95 (2008) 3802.
[31] K.A. Scott, P.J. Bond, A. Ivetac, A.P. Chetwynd, S. Khalid, M.S.P. Sansom, Structure 16 (2008) 621.
[32] T. Carpenter, P.J. Bond, S. Khalid, M.S.P. Sansom, Biophys. J. 95 (2008) 3790.
[33] M.S.P. Sansom, K.A. Scott, P.J. Bond, Biochem. Soc. Trans. 36 (2008) 27.
[34] R.S.G. D'Rozario, C.L. Wee, E.J. Wallace, M.S.P. Sansom, Nanotechnology (2009) 20.
[35] H.J. Risselada, S.J. Marrink, PNAS 105 (2008) 17367.
[36] E. Lindahl, B. Hess, D. van der Spoel, J. Mol. Model. 7 (2001) 306.
[37] D. Van der Spoel, E. Lindahl, B. Hess, G. Groenhof, A.E. Mark, H.J.C. Berendsen, J. Comput. Chem. 26 (2005) 1701.
[38] H.J.C. Berendsen, J.P.M. Postma, W.F. Vangunsteren, A. Dinola, J.R. Haak, J. Chem. Phys. 81 (1984) 3684.
[39] S.J. Marrink, A.H. de Vries, A.E. Mark, J. Phys. Chem. B 108 (2004) 750.
[40] W. Humphrey, A. Dalke, K. Schulten, J. Mol. Graph. 14 (1996) 33.
[41] D. Flock, G. Rossetti, I. Daidone, A. Amadei, A. Di Nola, Proteins – Struct. Funct. Bioinform. 65 (2006) 914.
[42] E. Cohen, J. Bieschke, R.M. Perciavalle, J.W. Kelly, A. Dillin, Science 313 (2006) 1604.